

Constraints on cosmology and gravity from the dynamics of voids

Nico Hamaus,^{1,*} Alice Pisani,^{2,3,4} P. M. Sutter,^{5,6,7} Guilhem Lavaux,^{3,4}
Stéphanie Escoffier,² Benjamin D. Wandelt,^{3,4,8} and Jochen Weller^{1,9,10}

¹*Universitäts-Sternwarte München, Fakultät für Physik,*

Ludwig-Maximilians Universität, Scheinerstr. 1, D-81679 München, Germany

²*Aix Marseille Université, CNRS/IN2P3, CPPM, UMR 7346, 163 avenue de Luminy, F-13288, Marseille, France*

³*Sorbonne Universités, UPMC Univ Paris 06, UMR 7095,*

Institut d'Astrophysique de Paris, 98 bis boulevard Arago, F-75014, Paris, France

⁴*CNRS, UMR 7095, Institut d'Astrophysique de Paris, 98 bis boulevard Arago, F-75014, Paris, France*

⁵*Center for Cosmology and AstroParticle Physics, Ohio State University,*

191 West Woodruff Avenue, Columbus, OH 43210, U.S.A.

⁶*INFN - National Institute for Nuclear Physics, via Valerio 2, I-34127 Trieste, Italy*

⁷*INAF - Osservatorio Astronomico di Trieste, via Tiepolo 11, I-34143 Trieste, Italy*

⁸*Departments of Physics and Astronomy, University of Illinois at Urbana-Champaign,*

1110 West Green Street, Urbana, IL 61801, U.S.A.

⁹*Max Planck Institute for Extraterrestrial Physics, Giessenbachstr. 1, D-85748 Garching, Germany*

¹⁰*Excellence Cluster Universe, Boltzmannstr. 2, D-85748 Garching, Germany*

The universe is mostly composed of large and relatively empty domains known as cosmic voids, whereas its matter content is predominantly distributed along their boundaries. The remaining material inside them, either dark or luminous matter, is attracted to these boundaries and causes voids to expand faster and to grow emptier over cosmic time. Using clustering statistics centered on voids identified in the CMASS galaxy sample from the Sloan Digital Sky Survey (SDSS), we constrain the matter density and gravitational growth of cosmic structure at a median redshift $\bar{z} = 0.57$. Our analysis models the detailed anisotropic shape of stacked voids in redshift space which arises from the dynamics of galaxies in their interior and vicinity. Adopting minimal assumptions on the statistical distribution and motion of these galaxies, we constrain the average matter content in the universe, as well as the linear growth rate of structure to be $\Omega_m = 0.281 \pm 0.031$ and $f/b = 0.417 \pm 0.089$ (68% c.l.), where b is the galaxy bias. These measurements are robust to a battery of consistency tests. They improve on existing constraints by accessing smaller-scale clustering information in galaxy surveys through an accurate model of non-linear dynamics in void environments. As such, our analysis furnishes a powerful probe of deviations from Einstein's general relativity in the low density regime which has largely remained untested so far. We find no evidence for such deviations in the data at hand.

After the epoch of recombination the initially tiny Gaussian density perturbations in the early universe have evolved increasingly nonlinear under the influence of gravity, generating what is known as the *cosmic web*. Because the gravitational force is attractive, structures with densities above the mean always contract, while underdense ones expand. The latter are referred to as *cosmic voids* and have progressively occupied most of the available space in our universe. While the dominant matter content of the universe is invisible (dark), luminous tracers such as galaxies allow observing this process directly via their peculiar motions that follow the dynamics of voids. Although the individual velocity of galaxies cannot be determined in most cases, its line-of-sight component causes a Doppler shift in their spectrum, in addition to the Hubble redshift of each galaxy. This leads to a unique pattern of *redshift-space distortions* (RSD) in the distribution of galaxies around void centers, which allows inferring their velocity flow statistically [1–3]. The relation between galaxy density and velocity in voids can then be used to test the predictions of general relativ-

ity on cosmological scales [4]. So far most studies have focused on correlations between galaxies in this context, but in the dynamics of voids non-linearities are less severe [4, 5]. As a consequence a large amount of smaller-scale information is unlocked for cosmological inference, resulting in a substantial decrease of statistical errors.

Another type of distortion in the distribution of galaxies can be generated by the so-called *Alcock-Paczynski* (AP) effect [6]. Galaxy surveys measure the redshifts δz and angles $\delta\vartheta$ between any two galaxies on the sky, but these can only be converted to the correct comoving distances r_{\parallel} parallel, and r_{\perp} perpendicular to the line of sight, if the expansion history and the geometry of the universe is known:

$$r_{\parallel} = \frac{c}{H(z)}\delta z, \quad r_{\perp} = D_A(z)\delta\vartheta. \quad (1)$$

The expansion history is described by the Hubble rate

$$H(z) = H_0\sqrt{\Omega_m(1+z)^3 + \Omega_k(1+z)^2 + \Omega_\Lambda}, \quad (2)$$

and the geometry by the angular diameter distance

$$D_A(z) = \frac{c}{H_0\sqrt{-\Omega_k}} \sin\left(H_0\sqrt{-\Omega_k} \int_0^z \frac{1}{H(z')} dz'\right). \quad (3)$$

* hamaus@usm.lmu.de

These, in turn, depend on the Hubble constant H_0 , the matter and energy content Ω_m and Ω_Λ , as well as the curvature Ω_k of the universe today. Therefore, a spherically symmetric structure may appear as an ellipsoid when incorrect cosmological parameters are assumed. The correct parameters can be obtained by demanding the average shape of cosmic voids to be spherically symmetric [7–11], i.e. the ellipticity

$$\varepsilon := \frac{r_{\parallel}}{r_{\perp}} = \frac{D_A^{\text{true}}(z)H^{\text{true}}(z)}{D_A^{\text{fid}}(z)H^{\text{fid}}(z)}, \quad (4)$$

to be unity for any galaxy that is located on a sphere of radius $r = (r_{\parallel}^2 + r_{\perp}^2)^{1/2}$ around its nearest void center. Here we distinguish between the unknown true, and the assumed fiducial values of D_A and H .

In this paper we apply these two concepts to voids identified in the distribution of galaxies observed with a redshift survey. Thereby, we closely follow the methodology presented in ref. 4, which has been tested on simulated mock-galaxy catalogs extensively. The starting point is the *Gaussian streaming model* [12], providing the average distribution of galaxies around voids (in short: void stack) in redshift space via their cross-correlation function

$$1 + \xi_{\text{vg}}(\mathbf{r}) = \int \frac{1 + b\delta_v(r)}{\sqrt{2\pi}\sigma_v} \exp\left[-\frac{(v_{\parallel} - v_v(r)\frac{r_{\parallel}}{r})^2}{2\sigma_v^2}\right] dv_{\parallel}. \quad (5)$$

Here, r and v denote void-centric distances and velocities of galaxies in real space. Because distances are observed in redshift space, one has to take into account the contribution from peculiar motions,

$$r_{\parallel} = \tilde{r}_{\parallel} - \frac{v_{\parallel}}{H(z)}(1+z), \quad (6)$$

where the tilde symbol indicates redshift space. Moreover, b describes the linear bias parameter for galaxies and σ_v their velocity dispersion. The radial density profile of voids in real space can be parametrized with an empirical fitting function obtained from simulations, such as given in ref. 5:

$$\delta_v(r) = \delta_c \frac{1 - (r/r_s)^{\alpha}}{1 + (r/r_v)^{\beta}}, \quad (7)$$

with a central under-density δ_c , scale radius r_s , slopes α and β , and the effective void radius r_v . The latter is not a free parameter, but determined via $r_v = (3V_v/4\pi)^{1/3}$, where V_v is the total volume of a void. The velocity profile can be obtained via mass conservation [13]. Up to linear order, it is given by

$$v_v(r) = -\frac{f(z)H(z)}{(1+z)r^2} \int_0^r \delta_v(q)q^2 dq, \quad (8)$$

where $f(z)$ is the linear growth rate of density perturbations. Assuming general relativity and a flat Λ CDM

cosmology it can be expressed as [14]

$$f(z) \simeq \left[\frac{\Omega_m(1+z)^3}{\Omega_m(1+z)^3 + \Omega_\Lambda} \right]^{0.55}. \quad (9)$$

Theories of modified gravity predict deviations from general relativity – and thus eq. (9) – to be most pronounced in unscreened low-density environments [15], potentially making voids a smoking gun for the detection of a fifth force. Note that the parameters (f, b, δ_c) are mutually degenerate in this model, but the combinations f/b and $b\delta_c$ can be constrained independently.

Our results are shown in fig. 1 for cosmic voids identified in the SDSS DR11 at a median redshift $\bar{z} = 0.57$ (see appendix for details). The different panels show void stacks of increasing effective void radius from left to right and top to bottom. Deviations from spherical symmetry are significant and clearly visible even by eye. These are due to RSD caused by peculiar velocities in the statistical distribution of galaxies around voids. On large enough scales most galaxies are attracted coherently by overdensities of the matter distribution and do not change directions, which leads to the characteristic compression of the ridge feature around the void centers along the line of sight, and is known as the *Kaiser effect* [16]. On smaller scales the velocity dispersion of galaxies becomes dominant over their coherent flow, causing an elongation of structures along the line of sight that opposes the latter, it is commonly referred to as *Finger-of-God* (FoG) effect. However, the scales considered in this analysis are still large enough for the Kaiser effect to be the dominant one, as evident in fig. 1.

In order to compare our model from eq. (5) with the observational data, we employ a Markov Chain Monte Carlo (MCMC) technique (see appendix). The best-fit solutions are shown as white contour levels in fig. 1 and the posterior distributions in the $\Omega_m - f/b$ plane for the individual void stacks are shown in fig. 2. A number of interesting features can be noted: first of all the constraints become tighter towards larger voids, although each stack contains the same number of them. However, large void stacks are sampled by many more galaxies than small ones, resulting in smaller statistical fluctuations in the data. In general a very reasonable agreement with our assumed fiducial cosmology is achieved, especially for intermediate-size voids within the range $30h^{-1}\text{Mpc} \lesssim r_v \lesssim 60h^{-1}\text{Mpc}$. On smaller scales the effects of nonlinear RSD (FoG) and scale-dependent galaxy bias may cause systematic deviations that are not accounted for in our model. On the other hand, our largest void stack necessarily exhibits the widest range of void sizes, as the void abundance drops exponentially in this regime. Therefore, both the RSD signal and the void profile get smeared over a wider range of scales, which can result in a biased fit. Nevertheless, the posteriors on Ω_m and f/b are all consistent with each other across a wide range of scales, providing largely independent and competitive constraints to the existing literature.

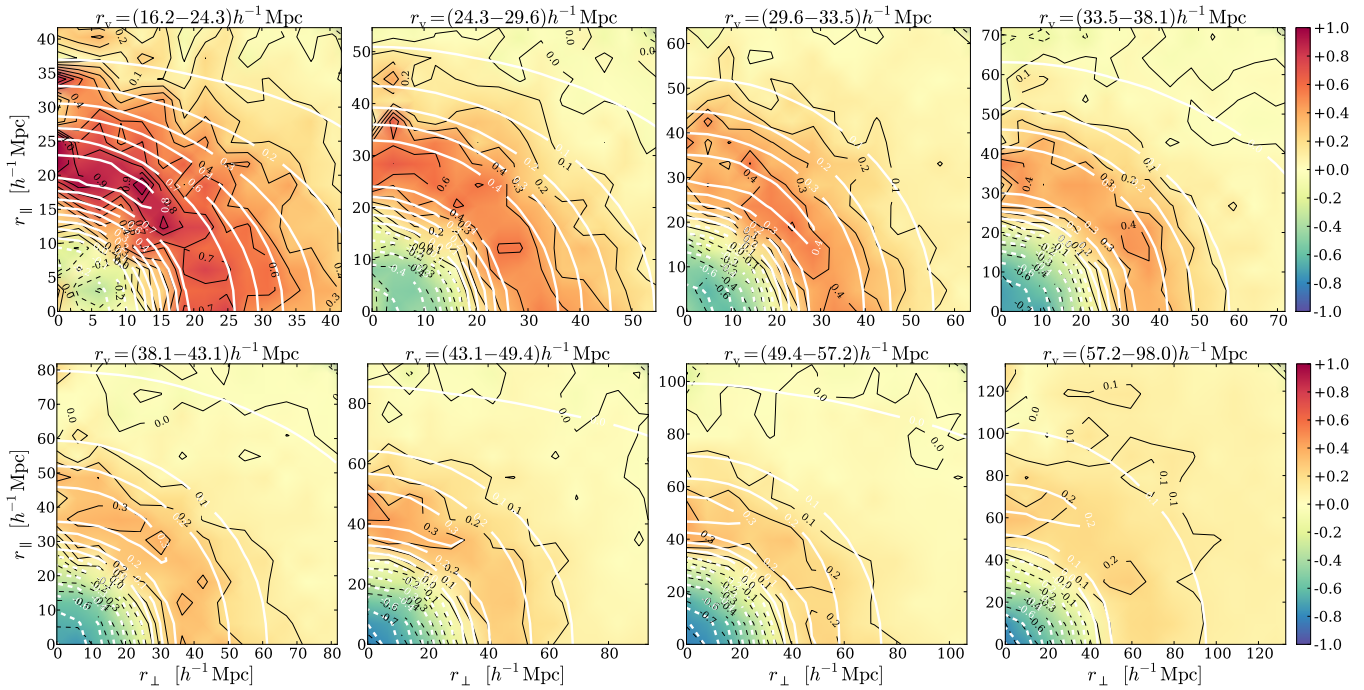


FIG. 1. Void stacks from the SDSS-III DR11 CMASS galaxies at $\bar{z} = 0.57$ in bins of increasing effective void radius r_v . Void centers are at the origin and the statistical distribution of galaxies in void-centric distances along and perpendicular to the line of sight (r_{\parallel} , r_{\perp}) are color-coded: red means more, blue fewer galaxies than average. By construction the average is set to zero (yellow). Black solid/dashed lines show positive/negative contours of the data, white lines show the maximum-likelihood fit of the model. Due to the symmetry of the stacks, only one quadrant is shown. The enhanced ridge feature along r_{\parallel} is caused by the coherent outflow of galaxies from the interior of voids. This allows to infer the strength of gravity (growth rate f/b) when compared to directions perpendicular to the line of sight r_{\perp} .

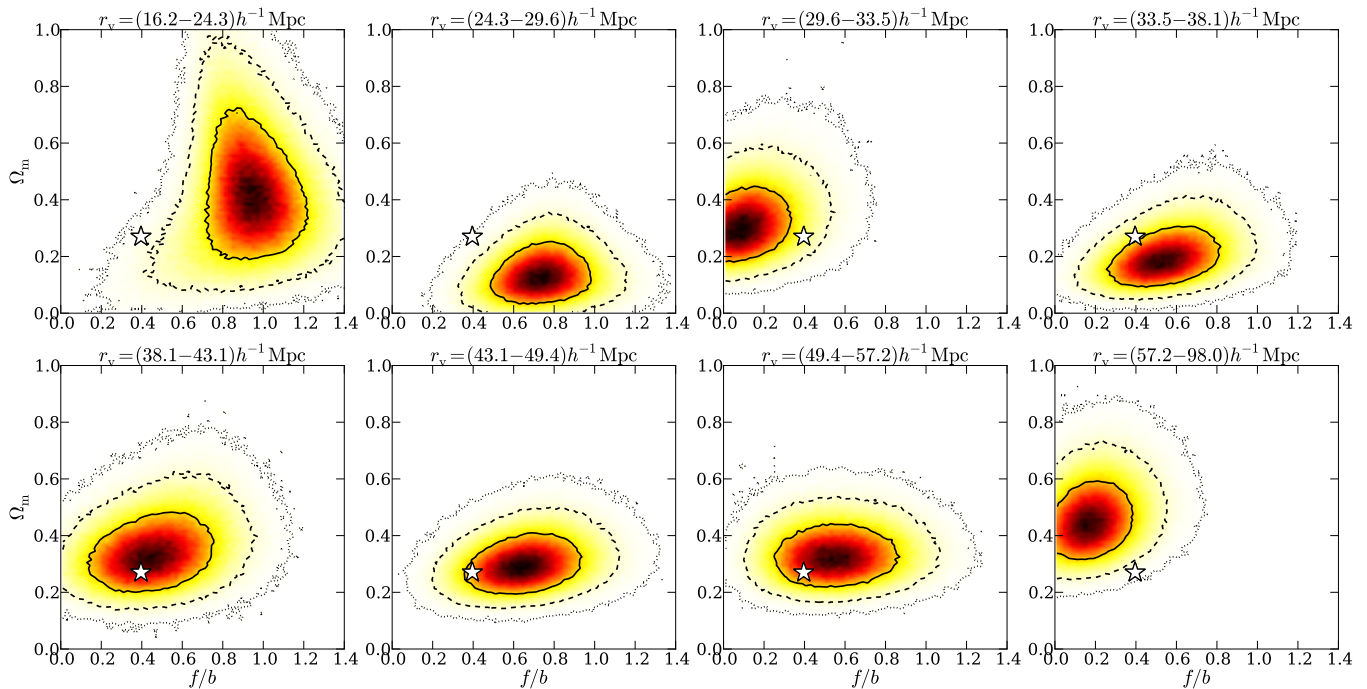


FIG. 2. Constraints on matter density Ω_m and growth rate f/b from each individual void stack of fig. 1. Solid, dashed, and dotted contour lines represent 68.3%, 95.5%, and 99.7% credible regions, respectively. Stars indicate fiducial values of $\Omega_m = 0.27$ and $f/b = 0.40$.

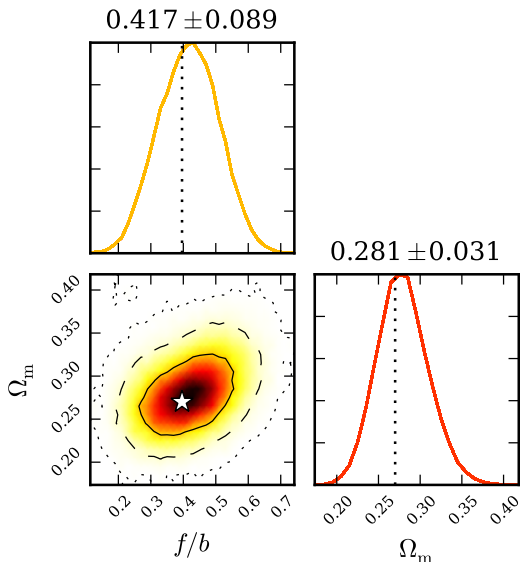


FIG. 3. Joint constraints on matter density Ω_m and growth rate f/b from all void stacks at $\bar{z} = 0.57$ combined. Their mean and standard deviation is shown above the marginal distributions. The star and dotted lines indicate fiducial values of $\Omega_m = 0.27$ and $f/b = 0.40$.

This is particularly the case when we choose to combine all the void stacks and infer the posterior parameter distribution jointly in a single MCMC chain that takes into account all the data at once. The resulting posterior distribution is presented in fig. 3, including the marginal distributions for both Ω_m and f/b individually. Our fiducial cosmology consistently falls inside the innermost confidence level of their joint posterior, and the standard deviation from the marginal distributions amounts to $\sim 11\%$ for Ω_m and $\sim 21\%$ for f/b , relative to their mean values. This implies a $\sim 1\%$ precision on the AP-parameter ε from eq. (4), which is about a factor of 4 smaller than current state-of-the-art galaxy clustering constraints from RSD (e.g. ref. 17), but obtained from a different regime of large-scale structure (see appendix for further checks). Moreover, so far we have neglected the large-scale regime of the void-galaxy cross-correlation function. It exhibits the baryon acoustic oscillation (BAO) feature, a relic clustering excess from the very early universe. The latter provides a standard ruler and allows breaking the degeneracy between $D_A(z)$ and $H(z)$ in eq. (4), resulting in even tighter cosmological constraints. The BAO feature in the clustering statistics of cosmic voids has recently been detected in the same data [18], a combined analysis with RSD therefore seems promising.

Our analysis demonstrates that a substantial amount of unexplored cosmological information can be made available through the analysis of cosmic voids. Besides their dynamics studied in this paper, voids also act as gravitational lenses [19–21], exhibit rich clustering statistics [22–24] including the BAO feature [18], and constrain

cosmology through their abundance and shapes [25, 26]. These complementary cosmological observables break parameter degeneracies and are promising probes of dark energy, general relativity [27–29], or the impact of massive neutrinos [30] on cosmological scales. We leave further investigations along these lines to the near future.

-
- [1] Padilla, N. D., Ceccarelli, L. & Lambas, D. G. Spatial and dynamical properties of voids in a Λ cold dark matter universe. *Mon. Not. R. Astron. Soc.* **363**, 977–990 (2005). astro-ph/0508297.
 - [2] Paz, D., Lares, M., Ceccarelli, L., Padilla, N. & Lambas, D. G. Clues on void evolution-II. Measuring density and velocity profiles on SDSS galaxy redshift space distortions. *Mon. Not. R. Astron. Soc.* **436**, 3480–3491 (2013). 1306.5799.
 - [3] Micheletti, D. *et al.* The VIMOS Public Extragalactic Redshift Survey. Searching for cosmic voids. *Astron. Astrophys.* **570**, A106 (2014). 1407.2969.
 - [4] Hamaus, N., Sutter, P. M., Lavaux, G. & Wandelt, B. D. Probing cosmology and gravity with redshift-space distortions around voids. *J. Cosmol. Astropart. Phys.* **11**, 36 (2015). 1507.04363.
 - [5] Hamaus, N., Sutter, P. M. & Wandelt, B. D. Universal Density Profile for Cosmic Voids. *Phys. Rev. Lett.* **112**, 251302 (2014). 1403.5499.
 - [6] Alcock, C. & Paczynski, B. An evolution free test for non-zero cosmological constant. *Nature* **281**, 358 (1979).
 - [7] Lavaux, G. & Wandelt, B. D. Precision Cosmography with Stacked Voids. *Astrophys. J.* **754**, 109 (2012). 1110.0345.
 - [8] Sutter, P. M., Lavaux, G., Wandelt, B. D. & Weinberg, D. H. A First Application of the Alcock-Paczynski Test to Stacked Cosmic Voids. *Astrophys. J.* **761**, 187 (2012). 1208.1058.
 - [9] Pisani, A., Lavaux, G., Sutter, P. M. & Wandelt, B. D. Real-space density profile reconstruction of stacked voids. *Mon. Not. R. Astron. Soc.* **443**, 3238–3250 (2014). 1306.3052.
 - [10] Sutter, P. M., Pisani, A., Wandelt, B. D. & Weinberg, D. H. A measurement of the Alcock-Paczynski effect using cosmic voids in the SDSS. *Mon. Not. R. Astron. Soc.* **443**, 2983–2990 (2014). 1404.5618.
 - [11] Hamaus, N., Sutter, P. M., Lavaux, G. & Wandelt, B. D. Testing cosmic geometry without dynamic distortions using voids. *J. Cosmol. Astropart. Phys.* **12**, 13 (2014). 1409.3580.
 - [12] Fisher, K. B. On the Validity of the Streaming Model for the Redshift-Space Correlation Function in the Linear Regime. *Astrophys. J.* **448**, 494 (1995). astro-ph/9412081.
 - [13] Peebles, P. J. E. *The large-scale structure of the universe* (Princeton University Press, Princeton, New Jersey, U.S.A., 1980).
 - [14] Linder, E. V. Cosmic growth history and expansion history. *Phys. Rev. D* **72**, 043529 (2005). astro-ph/0507263.
 - [15] Clifton, T., Ferreira, P. G., Padilla, A. & Skordis, C. Modified gravity and cosmology. *Phys. Rep.* **513**, 1–189 (2012). 1106.2476.
 - [16] Kaiser, N. Clustering in real space and in redshift space. *Mon. Not. R. Astron. Soc.* **227**, 1–21 (1987).

- [17] Gil-Marín, H. *et al.* The clustering of galaxies in the SDSS-III Baryon Oscillation Spectroscopic Survey: RSD measurement from the LOS-dependent power spectrum of DR12 BOSS galaxies. *ArXiv e-prints* (2015). 1509.06386.
- [18] Kitaura, F.-S. *et al.* Signatures of the primordial Universe from its emptiness. *ArXiv e-prints* (2015). 1511.04405.
- [19] Melchior, P., Sutter, P. M., Sheldon, E. S., Krause, E. & Wandelt, B. D. First measurement of gravitational lensing by cosmic voids in SDSS. *Mon. Not. R. Astron. Soc.* **440**, 2922–2927 (2014). 1309.2045.
- [20] Clampitt, J. & Jain, B. Lensing measurements of the mass distribution in SDSS voids. *Mon. Not. R. Astron. Soc.* **454**, 3357–3365 (2015). 1404.1834.
- [21] Gruen, D. *et al.* Weak lensing by galaxy troughs in DES Science Verification data. *Mon. Not. R. Astron. Soc.* **455**, 3367–3380 (2016). 1507.05090.
- [22] Hamaus, N., Wandelt, B. D., Sutter, P. M., Lavaux, G. & Warren, M. S. Cosmology with Void-Galaxy Correlations. *Phys. Rev. Lett.* **112**, 041304 (2014). 1307.2571.
- [23] Chan, K. C., Hamaus, N. & Desjacques, V. Large-scale clustering of cosmic voids. *Phys. Rev. D* **90**, 103521 (2014).
- [24] Clampitt, J., Jain, B. & Sánchez, C. Clustering and bias measurements of SDSS voids. *Mon. Not. R. Astron. Soc.* **456**, 4425–4431 (2016). 1507.08031.
- [25] Biswas, R., Alizadeh, E. & Wandelt, B. D. Voids as a precision probe of dark energy. *Phys. Rev. D* **82**, 023002 (2010). 1002.0014.
- [26] Pisani, A. *et al.* Counting voids to probe dark energy. *Phys. Rev. D* **92**, 083531 (2015). 1503.07690.
- [27] Cai, Y.-C., Padilla, N. & Li, B. Testing gravity using cosmic voids. *Mon. Not. R. Astron. Soc.* **451**, 1036–1055 (2015). 1410.1510.
- [28] Zivick, P., Sutter, P. M., Wandelt, B. D., Li, B. & Lam, T. Y. Using cosmic voids to distinguish f(R) gravity in future galaxy surveys. *Mon. Not. R. Astron. Soc.* **451**, 4215–4222 (2015). 1411.5694.
- [29] Barreira, A., Cautun, M., Li, B., Baugh, C. M. & Pascoli, S. Weak lensing by voids in modified lensing potentials. *J. Cosmol. Astropart. Phys.* **8**, 28 (2015). 1505.05809.
- [30] Massara, E., Villaescusa-Navarro, F., Viel, M. & Sutter, P. M. Voids in massive neutrino cosmologies. *J. Cosmol. Astropart. Phys.* **11**, 18 (2015). 1506.03088.

Acknowledgments We thank D. Paz, A. Hawken, B. Hoyle, and M.-C. Cousinou for discussions. Computations were performed on the HORIZON cluster at IAP. This work was supported by the ILP LABEX (ANR-10-LABX-63), French state funds managed by the ANR within the “Investissements d’Avenir” program (ANR-11-IDEX-0004-02), and NSF AST 09-08693 ARRA. N.H. and J.W. acknowledge support from the DFG cluster of excellence “Origin and Structure of the Universe”. A.P. acknowledges financial support from the grant OMEGA ANR-11-JS56-003-01 and support of the OCEVU LABEX (ANR-11-LABX-0060) and the A*MIDEX project (ANR-11-IDEX-0001-02) funded by the “Investissements d’Avenir” French government program managed by the ANR. P.M.S. is supported by the INFN IS PD51 “Indark”. B.D.W. is supported by a senior Excellence Chair by the Agence Nationale de Recherche (ANR-10-CEXC-004-01) and a Chaire Internationale at the Université Pierre et Marie Curie. J.W. also acknowledges support from the Trans-Regional Collaborative Research Center TRR 33 “The Dark Universe” of the Deutsche Forschungsgemeinschaft (DFG).

Funding for SDSS-III has been provided by the Alfred P. Sloan Foundation, the Participating Institutions, the National Science Foundation, and the U.S. Department of Energy Office of Science. The SDSS-III web site is www.sdss3.org. SDSS-III is managed by the Astrophysical Research Consortium for the Participating Institutions of the SDSS-III Collaboration including the University of Arizona, the Brazilian Participation Group, Brookhaven National Laboratory, Carnegie Mellon University, University of Florida, the French Participation Group, the German Participation Group, Harvard University, the Instituto de Astrofísica de Canarias, the Michigan State/Notre Dame/JINA Participation Group, Johns Hopkins University, Lawrence Berkeley National Laboratory, Max Planck Institute for Astrophysics, Max Planck Institute for Extraterrestrial Physics, New Mexico State University, New York University, Ohio State University, Pennsylvania State University, University of Portsmouth, Princeton University, the Spanish Participation Group, University of Tokyo, University of Utah, Vanderbilt University, University of Virginia, University of Washington, and Yale University.

APPENDIX

Data. For our analysis we use public data from the Baryon Oscillation Spectroscopic Survey (BOSS) [31] of the SDSS-III [32], more precisely the CMASS galaxy sample from Data Release 11 (DR11) [33]. This sample is spread over a redshift range of $0.43 < z < 0.7$ with a median of $\bar{z} = 0.57$ inside a total volume of about $3.5h^{-3}\text{Gpc}^3$, with a peak number density of roughly $4 \times 10^{-4}h^3\text{Mpc}^{-3}$ and a linear bias parameter of $b \simeq 1.87$ [34]. The catalog is then split into nearly volume-limited samples in order to allow a robust identification of voids in each of them. We use the VIDE software [35] to generate void catalogs, it is based on the implementation of a *watershed* algorithm provided by the code ZOBOV [36]. A detailed description of this procedure can be found in refs. 37 and 38 for DR7 and DR9, and in ref. 39 for DR11. Whenever we apply coordinate transformations via eq. (1), we assume the following fiducial cosmological parameters: $\Omega_m = 0.27$, $\Omega_\Lambda = 0.73$, $\Omega_k = 0$, and $h = 0.70$. The resulting void catalogs provide us with the sky-coordinates and redshifts of each void's volume-weighted barycenter, as well as its effective radius r_v and volume V_v , among many other properties. We only consider voids that do not intersect with any survey boundaries. Besides insisting on r_v to be at least as large as the mean galaxy separation in the sample to avoid Poisson contamination, we apply no further post-processing cuts. This results in a catalog of 3457 voids with effective radius range $16.2h^{-1}\text{Mpc} < r_v < 98.0h^{-1}\text{Mpc}$. We split the full range of void radii into 8 adjacent bins such that every bin contains the same number of voids. In each bin, all void centers and their surrounding galaxies that are within a distance of $3r_v$ are aligned with the line-of-sight direction and stacked. Each stack is then histogrammed in two directions: the void-centric distances along and perpendicular to the line of sight, r_\parallel and r_\perp , which yields an estimator of the void-galaxy cross-correlation function in redshift space. For more details on this procedure we refer the reader to ref. 4.

Analysis. For the comparison of our model from eq. (5) with the observational data in fig. 1, we employ a MCMC technique using a *Metropolis-Hastings* sampler, implemented in the software package PyMC [40]. Assuming Gaussian statistics, the likelihood can be expressed as

$$\mathcal{L}(\hat{\xi}_{vg}|\theta) \propto \exp \left[-\frac{1}{2}(\hat{\xi}_{vg} - \xi_{vg})^\top \mathbf{C}^{-1}(\hat{\xi}_{vg} - \xi_{vg}) \right], \quad (10)$$

where a $\hat{\xi}_{vg}$ denotes the measured void-galaxy cross-correlation function, \mathbf{C} its covariance matrix, and $\theta = (r_s, \delta_c, \alpha, \beta, \sigma_v, f/b, \Omega_m)$ the parameter vector of our model. Furthermore, we assume $\Omega_k = 0$ and set $H_0 = 100 \frac{\text{km}}{\text{s}} h \text{Mpc}^{-1}$, while expressing all distances in units of $h^{-1}\text{Mpc}$. The remaining cosmological parameters n_s and σ_8 do not appear explicitly here, but

their influence is captured by the void density-profile parameters $(r_s, \delta_c, \alpha, \beta)$. The covariance matrix is estimated via Jackknife resampling of the voids in each stack, and inverted using the *tapering* technique [41] (details in ref. 4). Imposing uniform prior distributions with sufficiently wide ranges for our model parameters, we estimate their posterior distribution by running MCMC chains of $\mathcal{O}(10^6)$ samples. For every void stack, we evaluate a best-fit model from the parameter set in the chain that yields the highest likelihood, as depicted in fig. 1.

Discussion. In order to check for systematics in our measurement, we have conducted a number of tests. A potential problem can arise from the inclusion of voids whose effective radius is close to the mean galaxy separation in the survey, both because of Poisson contamination and the effects of nonlinear RSD (FoG) [42]. We repeated our analysis after removing all voids with effective radii below twice the average galaxy separation, i.e. $r_v \gtrsim 30h^{-1}\text{Mpc}$. However, the final cosmological constraints are hardly affected by this stricter size-cut, since the information content from the smaller voids is relatively weak anyway, as can be seen in fig. 2.

As a further test concerning the significance of our results we considered bootstrap resampling of our original void catalog, i.e. randomly selecting the same number of voids with replacement. We generated 9 such bootstraps and repeated the inference process from all voids for each of the bootstrap realizations, the results are presented in fig. 4. The solid, dashed, and dotted contour levels correspond to 68.3%, 95.5%, and 99.7% confidence regions. Among all bootstraps, the fiducial parameters agree to 6/9 with the solid contour, to 8/9 with the dashed contour, and only 1/9 marginally lies outside the latter, but still within the dotted confidence level. Thus, the statistical fluctuations in the final constraints are entirely consistent with the expectation, providing further confidence in our constraints.

Last but not least, we cross-checked our measurement with the help of a simulated mock-galaxy catalog whose properties closely resemble the observed galaxy sample from this analysis. In particular, we used a common *halo occupation distribution* (HOD) model to populate dark matter halos from an N -body simulation with central and satellite galaxies, the HOD has been calibrated to the CMASS galaxies from the SDSS-III DR9 [43] resulting in a mean galaxy density of $3 \times 10^{-4}h^3\text{Mpc}^{-3}$ and a bias parameter of $b \simeq 1.84$. The simulation covers a cubic box of volume $1h^{-3}\text{Gpc}^3$ at redshift $z = 0.5$ and adopts a Planck 2013 cosmology [44] with $\Omega_m = 0.32$, $\Omega_\Lambda = 0.68$, $\Omega_k = 0$, and $h = 0.68$ (see ref. 4 for more details). From this mock-galaxy sample we identify 2559 voids and repeat our analysis with 9 different bootstraps from this catalog, the results of which are shown in fig. 5. The final parameter constraints and statistics are fully in line with the measurement from the observed data above. Again

we find 6 out of 9 bootstraps to agree with the input cosmology within the 68.3% confidence region, 8 out of 9 within the 95.5% one, leaving one bootstrap to agree only within 99.7% slightly outside the 95.5% contour level.

-
- [31] Dawson, K. S. *et al.* The Baryon Oscillation Spectroscopic Survey of SDSS-III. *Astron. J.* **145**, 10 (2013). 1208.0022.
 - [32] Eisenstein, D. J. *et al.* SDSS-III: Massive Spectroscopic Surveys of the Distant Universe, the Milky Way, and Extra-Solar Planetary Systems. *Astron. J.* **142**, 72 (2011). 1101.1529.
 - [33] Alam, S. *et al.* The Eleventh and Twelfth Data Releases of the Sloan Digital Sky Survey: Final Data from SDSS-III. *Astrophys. J. Suppl.* **219**, 12 (2015). 1501.00963.
 - [34] Anderson, L. *et al.* The clustering of galaxies in the SDSS-III Baryon Oscillation Spectroscopic Survey: baryon acoustic oscillations in the Data Releases 10 and 11 Galaxy samples. *Mon. Not. R. Astron. Soc.* **441**, 24–62 (2014). 1312.4877.
 - [35] Sutter, P. M. *et al.* VIDE: The Void IDentification and Examination toolkit. *Astron. Comput.* **9**, 1–9 (2015). 1406.1191.
 - [36] Neyrinck, M. C. ZOBOV: a parameter-free void-finding algorithm. *Mon. Not. R. Astron. Soc.* **386**, 2101–2109 (2008). 0712.3049.
 - [37] Sutter, P. M., Lavaux, G., Wandelt, B. D. & Weinberg, D. H. A Public Void Catalog from the SDSS DR7 Galaxy Redshift Surveys Based on the Watershed Transform. *Astrophys. J.* **761**, 44 (2012). 1207.2524.
 - [38] Sutter, P. M. *et al.* Voids in the SDSS DR9: observations, simulations, and the impact of the survey mask. *Mon. Not. R. Astron. Soc.* **442**, 3127–3137 (2014). 1310.7155.
 - [39] Pisani, A. *et al.* (2016). In preparation.
 - [40] Patil, A., Huard, D. & Fonnesbeck, C. J. PyMC: Bayesian Stochastic Modelling in Python. *J. Stat. Soft.* **35**, 1–81 (2010).
 - [41] Paz, D. J. & Sánchez, A. G. Improving the precision matrix for precision cosmology. *Mon. Not. R. Astron. Soc.* **454**, 4326–4334 (2015). 1508.03162.
 - [42] Pisani, A., Sutter, P. M. & Wandelt, B. D. Mastering the effects of peculiar velocities in cosmic voids. *ArXiv e-prints* (2015). 1506.07982.
 - [43] Manera, M. *et al.* The clustering of galaxies in the SDSS-III Baryon Oscillation Spectroscopic Survey: a large sample of mock galaxy catalogues. *Mon. Not. R. Astron. Soc.* **428**, 1036–1054 (2013). 1203.6609.
 - [44] PLANCK collaboration, P.A.R. Ade *et al.* Planck 2013 results. XVI. Cosmological parameters. *Astron. Astrophys.* **571**, A16 (2014). 1303.5076.

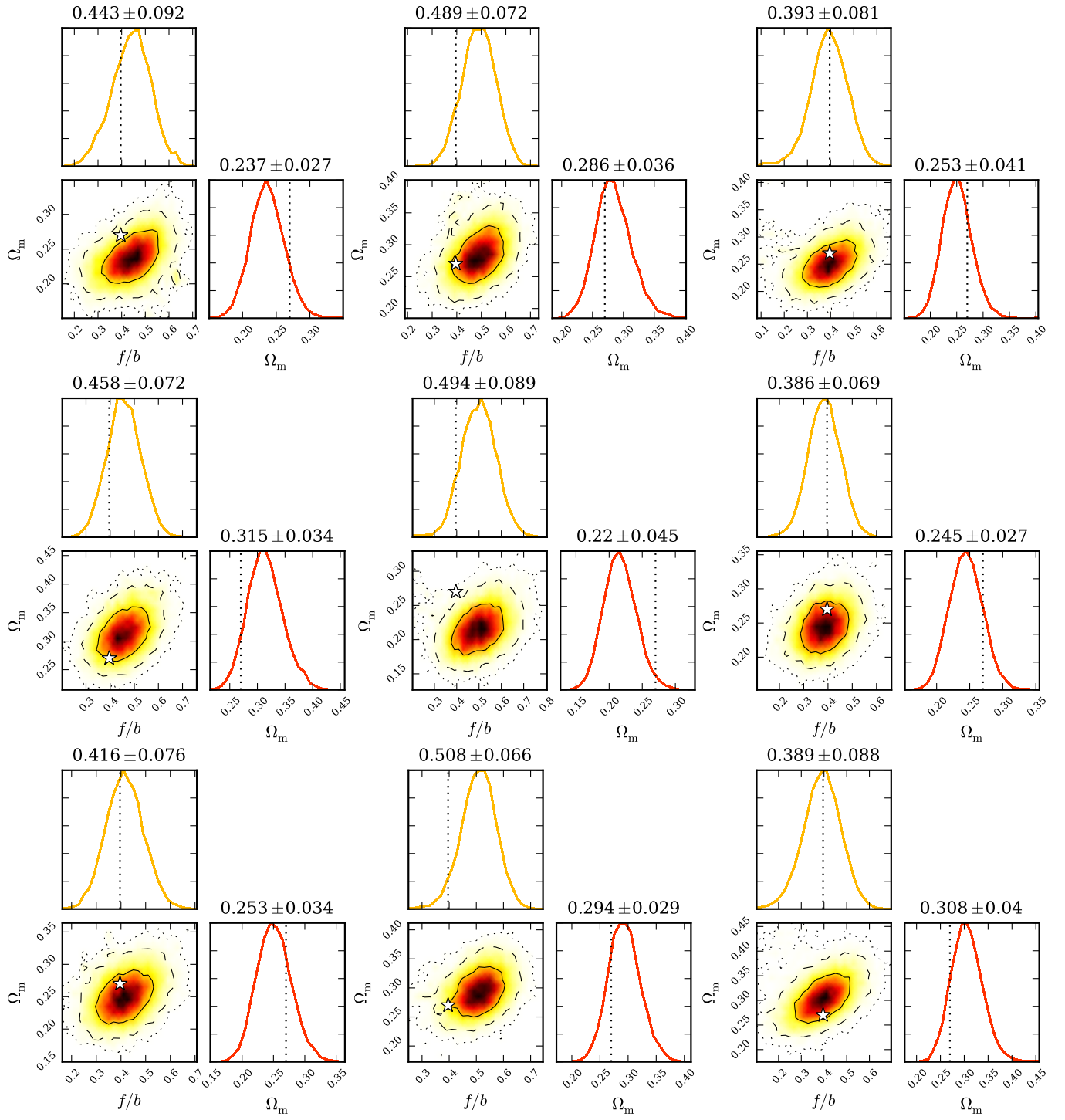


FIG. 4. Same as fig.3, but for 9 different bootstrap realizations of the original void catalog.

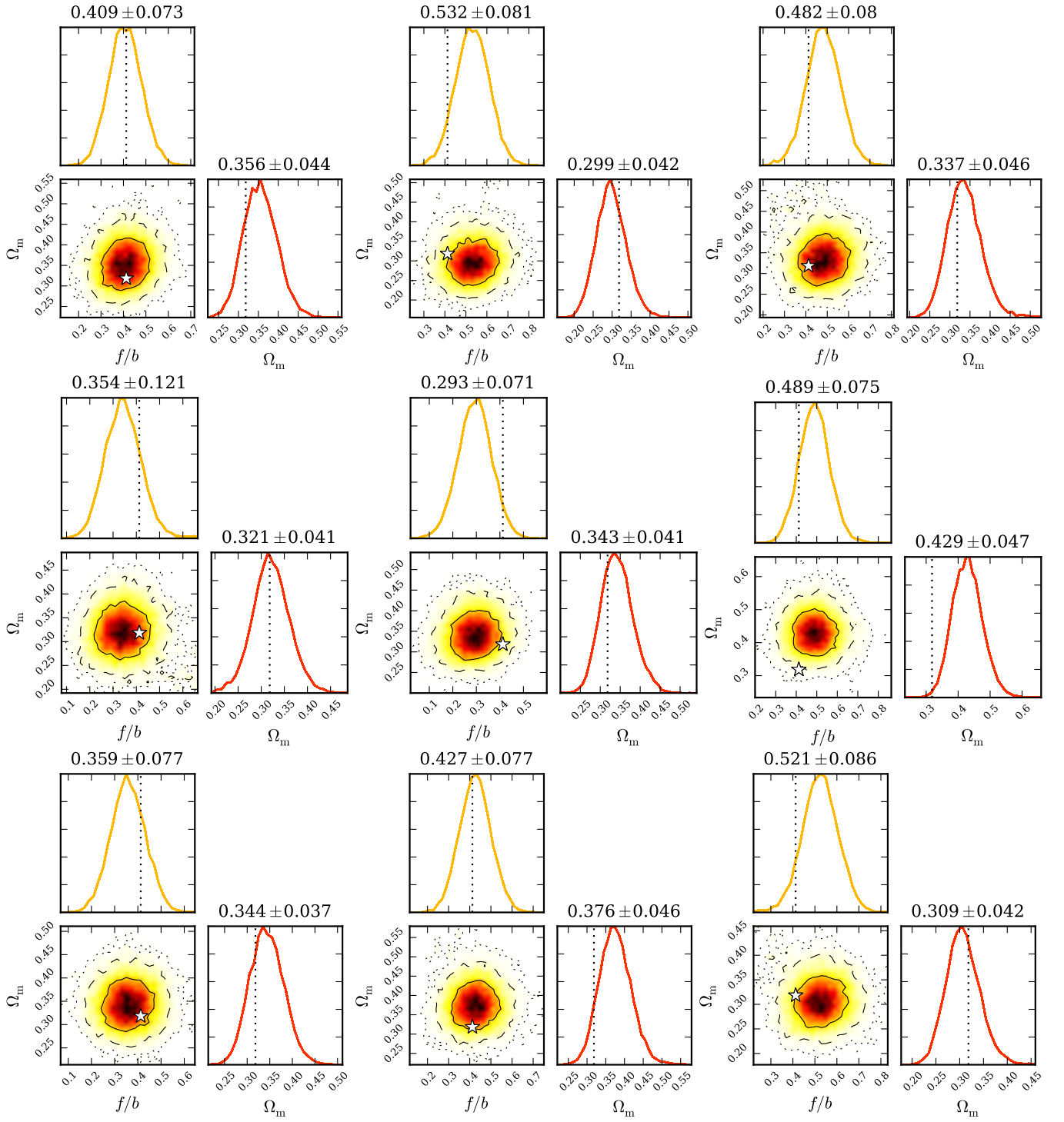


FIG. 5. Same as fig.3, but for 9 different bootstrap realizations of a mock void catalog with $\Omega_m = 0.32$ and $f/b = 0.41$.